Optical and magneto-optical properties of Bi substituted yttrium iron garnets prepared by metal organic decomposition

Eva Jesenska,[1,2,*] Tomohiko Yoshida,[1] Kenji Shinozaki,[1] Takayuki Ishibashi,[1] Lukas Beran,[2] Martin Zahradnik,[2] Roman Antos,[2] Miroslav Kučera,[2] and Martin Veis[2,3]

[1]*Department of Materials Science and Technology, Nagaoka University of Technology, Nagaoka, Niigata, 1603-1, Japan*
[2]*Institute of Physics, Charles University in Prague, Prague, 12116, Czech Republic*
[3]*veis@karlov.mff.cuni.cz*
[*]*jesenska@karlov.mff.cuni.cz*

Abstract: In this work, we present a systematic study of optical and magneto-optical properties of $Y_{3-x}Bi_xFe_5O_{12}$ thin films with various Bi concentrations ($x = 1.5, 2, 2.5, 3$) prepared by Metal Organic Decomposition on $Gd_3Ga_5O_{12}$ (100) substrates. We used magneto-optical spectroscopy and spectroscopic ellipsometry. Spectral dependence of complex refraction indexes obtained from ellipsometric measurements revealed increasing optical absorption with increasing Bi concentrations. Faraday and Kerr magneto-optical spectra measured in the photon energy range from 1.5 to 5.5 eV clearly demonstrated that the increasing Bi concentration enhances the spin-orbit coupling and influences the magneto-optical effect. Using the magneto-optical and ellipsometric experimental data we deduced a spectral dependence of complete permittivity tensor in a wide spectral range. Comparison of obtained results with the results reported on Liquid Phase Epitaxy bulk-like garnets with small Bi concentrations showed agreement and confirmed a high optical and magneto-optical quality of investigated films.

OCIS codes: (160.3820) Magneto-optical materials; (310.6860) Thin films, optical properties; (120.2130) Ellipsometry and polarimetry; (190.3270) Kerr effect; (230.2240) Faraday effect; (300.0300) Spectroscopy.

References and links

1. A. Kirihara, K. Uchida, Y. Kajiwara, M. Ishida, Y. Nakamura, T. Manako, E. Saitoh, and S. Yorozu, "Spin-current-driven thermoelectric coating," Nat. Mater. **11**(8), 686–689 (2012).
2. H. Nakayama, M. Althammer, Y.-T. Chen, K. Uchida, Y. Kajiwara, D. Kikuchi, T. Ohtani, S. Geprägs, M. Opel, S. Takahashi, R. Gross, G. E. W. Bauer, S. T. B. Goennenwein, and E. Saitoh, "Spin Hall Magnetoresistance Induced by a Nonequilibrium Proximity Effect," Phys. Rev. Lett. **110**(20), 206601 (2013).
3. H. Alisafaee and M. Ghanaatshoar, "Optimization of all-garnet magneto-optical magnetic field sensors with genetic algorithm," Appl. Opt. **51**(21), 5144–5148 (2012).
4. V. N. Berzhansky, T. V. Mikhailova, A. V. Karavainikov, A. R. Prokopov, A. N. Shaposhnikov, I. N. Lukienko, Y. N. Kharchenko, O. V. Miloslavskaya, and N. F. Kharchenko, "Microcavity One-Dimensional Magnetophotonic Crystals with Double Layer Iron Garnet," J. Phys. Soc. Jpn. **36**(1–2), 42–45 (2012).
5. L. Bi, J. Hu, P. Jiang, D. H. Kim, G. F. Dionne, L. C. Kimerling, and C. A. Ross, "On-chip optical isolation in monolithically integrated non-reciprocal optical resonators," Nat. Photonics **5**(12), 758–762 (2011).
6. A. B. Khanikaev and M. J. Steel, "Low-symmetry magnetic photonic crystals for nonreciprocal and unidirectional devices," Opt. Express **17**(7), 5265–5272 (2009).
7. S. Wittekoek, T. J. A. Poprna, J. M. Robertson, and P. F. Bongers, "Magneto-optic spectra and the dielectric tensor elements of bismuth-substituted iron garnets at photon energies between 2.2—5.2 eV," Phys. Rev. B **12**(7), 2777–2788 (1975).
8. M. Veis, E. Lišková, R. Antoš, Š. Višňovský, N. Kumar, D. S. Misra, N. Venkataramani, S. Prasad, and R. Krishnan, "Polar and longitudinal magneto-optical spectroscopy of bismuth substituted yttrium iron garnet films grown by pulsed laser deposition," Thin Solid Films **519**(22), 8041–8046 (2011).
9. P. Hansen and J.-P. Krumme, "Magnetic and magneto-optical properties of garnet films," Thin Solid Films **114**(1–2), 69–107 (1984).

10. C. F. Buhrer, "Faraday Rotation and Dichroism of Bismuth Calcium Vanadium Iron Garnet," J. Appl. Phys. **40**(11), 4500–4502 (1969).
11. C. F. Buhrer, "Enhancement of the Faraday Rotation of Iron Garnets by Bismuth and Rare-Earth Ions," J. Appl. Phys. **41**(3), 1393–1394 (1970).
12. S. Wittekoek and D. E. Lacklison, "Investigation of the Origin of the Anomalous Faraday Rotation of $Bi_xCa_{3-x}Fe_{3.5+0.5x}V_{1.5-0.5x}O_{12}$ by Means of the Magneto-optical Kerr Effect," Phys. Rev. Lett. **28**(12), 740–743 (1972).
13. H. Takeuchi, "The Faraday Effect of Bismuth Substituted Rare-Earth Iron Garnet," Jpn. J. Appl. Phys. **14**(12), 1903–1910 (1975).
14. M.-Y. Chern and J.-S. Liaw, "Study of $Bi_xY_{3-x}Fe_5O_{12}$ Thin Films Grown by Pulsed Laser Deposition," Jpn. J. Appl. Phys. **36**(1), 1049–1053 (1997).
15. J.-P. Krumme, V. Doormann, and P. Willich, "Bismuth iron garnet films prepared by rf magnetron sputtering," J. Appl. Phys. **57**(8), 3885–3887 (1985).
16. T. Okuda, N. Koshizuka, K. Hayashi, T. Takahashi, H. Kobani, and H. Yamamoto, "Faraday Rotation In Highly Bi-Substituted Yttrium Iron Garnet Films Prepared By Ion Beam Sputtering," IEEE Trans. Magn. **23**(5), 3491–3493 (1987).
17. M. Okada, S. Katayama, and K. Tominaga, "Preparation and magneto-optic properties of Bi-substituted yttrium iron garnet thin films by metalorganic chemical vapor deposition," J. Appl. Phys. **69**(6), 3566–3570 (1991).
18. H. Kidoh, A. Morimoto, and T. Shimizu, "Synthesis of ferromagnetic Bi-substituted yttrium iron garnet films by laser ablation," Appl. Phys. Lett. **59**(2), 237–239 (1991).
19. K. Matsumoto, S. Sasaki, Y. Asahara, K. Yamaguchi, and T. Fujii, "Highly bismuth substituted yttrium iron garnet single crystal films prepared by sol-gel method," J. Magn. Magn. Mater. **104–107**(1), 451–452 (1992).
20. V. J. Fratello, S. J. Licht, C. D. Brandle, H. M. O'Bryan, and F. A. Baiocchi, "Effect of bismuth doping on thermal expansion and misfit dislocations in epitaxial iron garnets," J. Cryst. Growth **142**(1–2), 93–102 (1994).
21. J.-L. Rehspringer, J. Bursik, D. Niznansky, and A. Klarikova, "Characterisation of bismuth-doped yttrium iron garnet layers prepared by sol-gel process," J. Magn. Magn. Mater. **211**(1–3), 291–295 (2000).
22. J. L. Deschanvres and D. Cenda, "Deposition of Bi-substituted iron garnet magneto-optic thin films by MOCVD," J. Magn. Magn. Mater. **242–245**(2), 1172–1174 (2002).
23. P. Papakonstantinou, B. Teggart, and R. Atkinson, "The effects of substrate temperature and oxygen pressure on pulsed laser deposited Bi-substituted Dy iron garnet films," J. Magn. Magn. Mater. **163**(3), 378–392 (1996).
24. N. Watanabe, N. Takahashi, and K. Tsushima, "Non-equilibrium garnet films grown by pulsed laser deposition," Mater. Chem. Phys. **54**(1–3), 173–176 (1998).
25. S. Kahl and A. M. Grishin, "Evolution of properties of epitaxial bismuthiron garnet films with increasing thickness," J. Magn. Magn. Mater. **278**(1–2), 244–255 (2004).
26. A. Hasanpoura, M. Mozaffaria, J. Amighiana, H. Richertd, A. Lorenzd, M. Lindnerd, P. Gornertd, and H. Heegn, "Preparation and magneto-optical properties of $BiY_2Fe_5O_{12}$ organic nanocomposite films," J. Magn. Magn. Mater. **317**(1–2), 41–45 (2007).
27. Q.-H. Yang, H.-W. Zhnag, Q.-Y. Wen, Y.-L. Liu, I. M. Syvorotka, and I. I. Syvorotka, "Magneto-optical and Microwave Properties of LuBiIG Thin Films Prepared by Liquid Phase Epitaxy Method from Lead-Free Flux," Chin. Phys. Lett. **26**(4), 047401 (2009).
28. S. Leitenmeier, T. Korner, J. Griesbauer, M. Herbort, A. Heinrich, and B. Stritzker, "Studies on the growth of epitaxial bismuth-substituted iron garneton gadolinium gallium garnet single crystals by pulsed laser deposition," J. Cryst. Growth **310**(24), 5392–5401 (2008).
29. T. Ishibashi, A. Mizusawa, M. Nagai, S. Shimizu, K. Sato, N. Togashi, T. Mogi, M. Houchido, H. Sano, and K. Kuriyama, "Characterization of epitaxial $(Y,Bi)_3(Fe,Ga)_5O_{12}$ thin films grown by metalorganic decomposition method," J. Appl. Phys. **97**(1), 013516 (2005).
30. V. Berzhansky, T. Mikhailova, A. Shaposhnikov, A. Prokopov, A. Karavainikov, V. Kotov, D. Balabanov, and V. Burkov, "Magneto-optics of nanoscale Bi:YIG films," Appl. Opt. **52**(26), 6599–6606 (2013).
31. Š. Višňovský, *Optics in Magnetic Multilayers and Nanostructures* (Taylor & Francis, 2006).
32. Š. Višňovský, "Magneto-Optical Effects In Crystals At The Normal Incidence," Czech. J. Phys. **37**(2), 218–231 (1987).
33. I. J.A. Woollam Co, CompleteEASE Data Analysis Manual (J.A. Woollam Co., Inc., 2011).
34. G. E. J. Jr and F. A. Modine, "Parameterization of the optical functions of amorphous materials in the interband region," Appl. Phys. Lett. **69**(3), 371–373 (1996).
35. B. Johsa, C. M. Herzingera, J. H. Dinan, A. Cornfeld, and J. D. Benson, "Development of a parametric optical constant model for $Hg_{1-x}Cd_xTe$ for control of composition by spectroscopic ellipsometry during MBE growth," Thin Solid Films **313–314**(1–2), 137–142 (1998).
36. D. D. S. Meneses, M. Malki, and P. Echegut, "Structure and lattice dynamics of binary lead silicate glasses investigated by infrared spectroscopy," J. Non-Cryst. Solids **352**(8), 769–776 (2006).
37. P. Yeh, "Optics Of Anisotropic Layered Media: A New 4 X 4 Matrix Algebra," Surf. Sci. **96**(1–3), 41–53 (1979).
38. D. Schmidt and M. Schubert, "Anisotropic Bruggeman Effective Medium Approaches for Slanted Columnar Thin Films," J. Appl. Phys. **114**(8), 083510 (2013).
39. T. Ishibashi, K. Kawata, T. H. Johansen, J. He, N. Harada, and K. Sato, "Magneto-optical Indicator Garnet Fimls Grown by Metal-organic Decomposition Method," J. Phys. Soc. Jpn. **32**(2-2), 150–153 (2008).
40. T. Ishibashi, T. Kosaka, M. Naganuma, and T. Nomura, "Magneto-optical properties of Bi-substituted yttrium iron garnet films by metal-organic decomposition method," *in Proceedings of International Conference on Magnetism (ICM 2009)*, (IOP Publishing, 2009), pp. 112002 (112004).

41. T. Ishibashi, G. Lou, A. Meguro, T. Hashinaka, M. Sasaki, and T. Nishi, "Magneto-optical Imaging Plate Using Bismuth-Substituted Iron Garnet Film Prepared by Metal-Organic Decomposition," Sens. Mater. **27**(10), 965–970 (2015).
42. H. Lee, Y. Yoon, S. Kim, H. K. Yoo, H. Melikyan, E. Danielyan, A. Babajanyan, T. Ishibashi, B. Friedman, and K. Lee, "Preparation of bismuth substituted yttrium iron garnet powder and thin film by the metal-organic decomposition method," J. Cryst. Growth **329**(1), 27–32 (2011).
43. P. Johansson, S. I. Khartsev, and A. M. Grishin, "Comparison of Bi3Fe5O12 film giant Faraday rotators grown on (111) and (001) Gd3Ga5O12 single crystals," Thin Solid Films **515**(2), 477–480 (2006).
44. S. Yao, T. Sato, K. Kaneko, S. Murai, K. Fujita, and K. Tanaka, "Faraday effect of bismuth iron garnet thin film prepared by mist CVD method," Jpn. J. Appl. Phys. **54**(6), 063001 (2015).
45. M. Deb, E. Popova, A. Fouchet, and N. Keller, "Magneto-optical Faraday spectroscopy of completely bismuth-substituted Bi₃Fe₅O₁₂ garnet thin films," J. Phys. D Appl. Phys. **45**(45), 455001 (2012).
46. E. Popova, N. Keller, F. Gendron, L. Thomas, M.-C. Brianso, M. Guyot, M. Tessier, and S. S. P. Parkin, "Perpendicular magnetic anisotropy in ultrathin yttrium iron garnet films prepared by pulsed laser deposition technique," J. Vac. Sci. Technol. **19**(5), 2567–2570 (2001).
47. E. Popova, N. Keller, F. Jomard, L. Thomas, M.-C. Brianso, F. Gendron, M. Guyot, and M. Tessier, "Exchange coupling in ultrathin epitaxial yttrium iron garnet films," EPJ B **31**(1), 69–74 (2003).
48. S. Zollner, A. A. Demkov, R. Liu, P. L. Fejes, R. B. Gregory, P. Alluri, J. A. Curless, Z. Yu, J. Ramdani, R. Droopad, T. E. Tiwald, J. N. Hilfiker, and J. A. Woollam, "Optical properties of bulk and thin-film SrTiO3 on Si and Pt," J. Vac. Sci. Technol. B **18**(4), 2242–2254 (2000).

1. Introduction

Magnetic garnets have attracted a considerable attention due to spintronic phenomena such as the spin Seebeck effect [1] and spin Hall magneto-resistance [2], or applications in integrated magneto-optical (MO) [3, 4] and non-reciprocal photonic devices [5, 6]. Yttrium iron garnets with high bismuth ion concentrations, $Y_{3-x}Bi_xFe_5O_{12}$ (Bi:YIGs) exhibit very strong spin-orbit coupling caused by the presence of Bi resulting into a high MO figure of merit [7–14]. Several techniques such as liquid phase epitaxy, pulse laser deposition, sol-gel method or metalorganic chemical vapor deposition have been used to grow Bi:YIGs films of high optical and MO quality [15–28]. Among them, metal organic decomposition (MOD) has demonstrated to be a very promising method, because it is inexpensive and guarantees highly uniform chemical composition and purity combined with chemical stability [29]. Moreover, MOD is advantageous because of the good productivity, since it involves simple processes performed in the air and it ensures a possibility of formation over a large area. Finally, MOD is an effective technique for the preparation of Bi:YIGs thin films with high Bi content ($x \geq 2$) (including the full substitution) which is usually rather complicated and possible only with a few non-equilibrium growth techniques [30]. A systematic optical and MO study of MOD Bi:YIGs thin films was not reported yet, although optical and MO properties are important indicators of the overall film quality.

The main purpose of our investigation in the present work was to fully determine the dielectric permittivity tensor of Bi:YIGs thin films. We used optical and MO spectral measurements at energies from 1.5 to 5 eV. Obtained results allowed us to compare the properties of investigated Bi:YIGs thin films prepared by MOD to properties of bulk-like Bi:YIGs with small Bi concentrations prepared by epitaxial growth [7, 9]. We examined optical properties by Spectroscopic Ellipsometry (SE) supported by transmission intensity measurements. From these data we derived the diagonal permittivity tensor elements. We examined MO properties by spectroscopic polar MO Kerr effect (MOKE) and Faraday rotation and ellipticity measurements. Using a combination of the SE results with MO measurements we determined the spectral dependence of off-diagonal permittivity tensor elements.

2. Theory

The behavior of electromagnetic waves in a material can be described by permittivity and permeability tensors. At optical frequencies, we can take magnetic permeability as unity. If we are working with a cubic crystal and magnetization parallel to the z-axis of the Cartesian coordinate system (the magnetic film-ambient interface is normal to the z-axis), the dielectric permittivity tensor has the form

$$\varepsilon = \begin{pmatrix} \varepsilon_1 & -i \cdot \varepsilon_2 & 0 \\ i \cdot \varepsilon_2 & \varepsilon_1 & 0 \\ 0 & 0 & \varepsilon_3 \end{pmatrix}. \tag{1}$$

In this work we restricted ourselves to linear MO effects, which implies $\varepsilon_3 = \varepsilon_1$ [31, 32]. All elements of the tensor have a real and imaginary part:

$$\begin{aligned} \varepsilon_1 &= \varepsilon_{1r} - i \cdot \varepsilon_{1i} \\ \varepsilon_2 &= \varepsilon_{2r} - i \cdot \varepsilon_{2i}. \end{aligned} \tag{2}$$

We can describe optical behavior of the sample upon both, light reflection and transmission, in the base of s and p polarization components by Jones reflection and transmission matrices [31,32]

$$J_{sp}^{R} = \begin{pmatrix} r_{ss} & r_{sp} \\ r_{ps} & r_{pp} \end{pmatrix} J_{sp}^{I}, \tag{3}$$

$$J_{sp}^{T} = \begin{pmatrix} t_{ss} & t_{sp} \\ t_{ps} & t_{pp} \end{pmatrix} J_{sp}^{I}, \tag{4}$$

Matrix elements are the amplitude reflection and transmission coefficients for the s and p polarized waves.

We can derive diagonal elements of the permittivity tensor from the SE data analysis. The change in the polarization state of the reflected beam can be expressed by ellipsometric Psi (ψ) and Delta (Δ) parameters defined by equation

$$\tan\psi \cdot e^{i\Delta} = \rho = \frac{r_{pp}}{r_{ss}}. \tag{5}$$

In this equation, $\tan\psi$ is the magnitude of the reflectivity ratio and Δ is the phase. The r_{pp} and r_{ss} are amplitude reflection coefficients for s and p polarization measured from the alternating current (AC) signal [33]. A common approach to increase the information content when measuring absorbing thin film on transparent substrate is to supplement the SE data with intensity transmission data (transmitted intensity is calculated from the AC signal). The important step in the SE analysis is the proper parametrization of the dispersion of the unknown optical functions. In this work, we used Kramers-Kronig (KK) consistent Tauc-Lorentz, general Herzinger-Johns and Gaussian parameterization. Tauc-Lorentz parameterization defines the imaginary part of the complex dielectric function as

$$\varepsilon_{1i} = \left[\frac{Amp E_0 Br(E - E_g)^2}{E(E^2 - E_0^2)^2 + Br^2 E^2} \right], \qquad E > E_g \tag{6}$$

$$\varepsilon_{1i} = 0, \qquad E \le E_g. \tag{7}$$

Parameters E_0, E_g, Amp, Br denote the center energy of oscillator, band gap energy, amplitude and the broadening parameter respectively [33, 34]. The ε_{1r} is obtained using analytical integration of KK relation. The Herzinger-Johns model utilizes four polynomials to accurately reproduce complicated shapes of dielectric functions. This model is primarily intended to fit dielectric functions of semiconductors and other crystalline materials. A detailed description can be found in [33, 35]. Finally, Gaussian oscillator produces Gaussian line shape in ε_{1i}:

$$\varepsilon_{1\_Gaussian} = Amp \left\{ \begin{bmatrix} \left(\Gamma\left(\dfrac{E-E_0}{\sigma}\right) + \Gamma\left(\dfrac{E+E_0}{\sigma}\right) \right) + \\ i \cdot \left(\exp\left[-\left(\dfrac{E-E_0}{\sigma}\right)^2 \right] + \exp\left[-\left(\dfrac{E+E_0}{\sigma}\right)^2 \right] \right) \end{bmatrix} \right\}, \qquad (8)$$

$$\sigma = \frac{Br}{2\sqrt{\ln(2)}}. \qquad (9)$$

The function Γ is a convergence series that produces a KK consistent line shape for ε_{1r} [33, 36].

With the knowledge of the diagonal elements of the permittivity tensor, we can derive the off-diagonal elements using a combination of MOKE and Faraday spectra along with theoretical calculations. These calculations are based on Yeh's 4x4 matrix formalism which is discussed in detail in [31, 32, 37]. We can express the change in a polarization state of the light upon reflection/transmission by the complex Kerr MO angle Φ_K and the complex Faraday MO angle Φ_F. These are for p-polarized incident light defined as follows

$$\Phi_K = \theta_K - i \cdot e_K = \frac{r_{sp}}{r_{pp}}, \qquad (10)$$

$$\Phi_F = \theta_F - i \cdot e_F = \frac{t_{sp}}{t_{pp}}. \qquad (11)$$

In these equations Θ_k is the Kerr rotation, e_k is the Kerr ellipticity, Θ_F is the Faraday rotation and e_F is the Faraday ellipticity. Here we define MO figure of merit as $2|\Theta_F|/\alpha$, where α is the absorption coefficient. Let us consider the case of a 2 layered medium, where the first layer is a bulk substrate and the second layer is a thin film. We will work in Cartesian coordinates where the sample interface is perpendicular to the z-axis, the wave vector of the incident light is perpendicular to the x-axis and each layer is characterized by a complex permittivity tensor and a thickness. In this case, Yeh Matrix Formalism allows to express the relationship between the electric field amplitudes on the substrate/film interface ($E_0^{(0)}(z)$) and the electric field amplitudes on the film/ambient interface ($E_0^{(2)}(z_1)$) as

$$E_0^{(0)}(z) = [D^{(0)}]^{-1} D^{(1)} P^{(1)} [D^{(1)}]^{-1} D^{(2)} E_0^{(2)}(z_1) = M E_0^{(2)}(z_1). \qquad (12)$$

Superscripts in brackets, n = 0, 1 and 2 are markers of the substrate (0), thin film (1) and the ambient half space (2). P stands for propagation matrix

$$P_{ij}^{(n)} = \delta_{ij} \exp(i \frac{\omega}{c} N_{zj}^{(n)} t_n) \qquad (13)$$

and D for dynamical matrix defined as

$$\begin{aligned}
D_{1j}^{(n)} &= -\varepsilon_2^{(n)}(\varepsilon_1^{(n)} - N_y^2) \\
D_{2j}^{(n)} &= N_{zj}^{(n)} D_{1j}^{(n)} \\
D_{3j}^{(n)} &= (\varepsilon_1^{(n)} - N_y^2)(\varepsilon_1^{(n)} - N_y^2 - (N_{zj}^{(n)})^2), \\
D_{4j}^{(n)} &= -\varepsilon_1^{(n)}(\varepsilon_1^{(n)} - N_y^2 - (N_{zj}^{(n)})^2)
\end{aligned} \qquad (14)$$

where t_n, N_{zj} and N_y are the thickness of the n-th layer, z components of the reduced wave vector and y component of the reduced wave vector respectively [31].

Model structure used in our SE, MOKE and Faraday effect analysis consisted of a semi-infinite GGG substrate and Bi:YIGs layer. We also considered surface roughness and GGG/Bi:YIG interface roughness. These were represented by thin layers with permittivities given by Bruggeman Effective Medium Approximation formula (BEMA). BEMA creates an effective dielectric permittivity ε_{eff} for a system made up of inclusions of a material with dielectric permittivity ε_m in a material with dielectric permittivity ε_h as follows:

$$(f-1)\frac{\varepsilon_h - \varepsilon_{eff}}{\varepsilon_{eff} + D(\varepsilon_h - \varepsilon_{eff})} = f\frac{\varepsilon_m - \varepsilon_{eff}}{\varepsilon_{eff} + D(\varepsilon_m - \varepsilon_{eff})}. \tag{15}$$

In this formula f denotes the volume fraction of the ε_m material inclusions ($f \in (0, 1)$) and D stands for depolarization fixed to 1/3, which corresponds to spherical inclusions [38].

3. Experimental details

3.1 MOD and sample characterization

In this work, we studied $Y_{3-x}Bi_xFe_5O_{12}$ thin films (x = 1.5, 2, 2.5, 3) prepared on $Gd_3Ga_5O_{12}$ (GGG) (100) substrates. Compositions of garnet films are listed in the Table 1. The thin films were prepared by MOD method. MOD liquids for garnet films consisted of solutions made of Bi, Y, and Fe carboxylates. The total concentration of carboxylates was 3 – 4% [39, 40]. We prepared MOD liquids by mixing each solution to obtain desired chemical compositions. We spin-coated those solutions on GGG (100) substrates with 3000 rpm for 60 s. This process was followed by drying at 100 °C for 30 minutes using a hot-plate. In order to decompose organic materials and to obtain amorphous oxide films, we pre-annealed samples at 450 °C for 30 minutes. We repeated this procedure, from spin coating to pre-annealing, 4-5 times in order to obtain appropriate thicknesses. Thin films examined in the present study had nominal thicknesses 160 and 200 nm (see Table 1). We determined nominal thicknesses from the number of MOD cycles calibrated by X-ray measurements. Finally, we annealed the samples for crystallization in a furnace at 700 °C for 3 hours. We performed all thermal treatments in the air. Further information on garnet films prepared by MOD method can be found in Ref [29].

Table 1. Composition and nominal thicknesses of examined garnet films

Film composition	Indication in figures and text	Nominal thickness (nm)
$Bi_3Fe_5O_{12}$	Bi3IG	200
$Y_{0.5}Bi_{2.5}Fe_5O_{12}$	Bi2.5YIG	160
$Y_1Bi_2Fe_5O_{12}$	Bi2YIG	200
$Y_{1.5}Bi_{1.5}Fe_5O_{12}$	Bi1.5YIG	200

3.2 Spectroscopic ellipsometry measurement

We performed SE measurements on a Mueller matrix ellipsometer Woollam RC2. We measured spectral dependence of ellipsometric parameters ψ and Δ in reflection and in the spectral range from 1.5 to 6.5 eV at incident angles 55°, 60° and 65°. We used the same equipment to measure the transmission spectra in the same spectral range at the incidence angle 0°.

3.3 Magneto-optical measurements

We studied MO properties of samples by MOKE and MO Faraday effect spectroscopy. We measured MOKE rotation and ellipticity spectra in the polar configuration using a method of generalized MO ellipsometry with rotating analyzer [32] allowing the determination of the rotation angles with precision better than 0.001 degree. We acquired the spectra of polar MOKE rotation and ellipticity at room temperature at nearly normal light incidence. Applied magnetic field was 1.2 T, which was enough for samples saturation. Incident light was p-polarized. We recorded data in the photon energy range from 1.4 to 5 eV.

We measured Faraday rotation and ellipticity spectra using the same experimental method. We acquired spectra of Faraday rotation and ellipticity at room temperature using magnetic field 665 mT, which was enough for samples saturation. We recorded experimental data in the photon energy range from 1.4 to 4 eV. Faraday hysteresis loops were measured at 3 eV.

4. Results and discussion

4.1 Spectroscopic ellipsometry

We analyzed SE experimental data using a CompleteEase software provided by Woollam Co.. We determined spectral dependences of optical parameters (diagonal elements of the permittivity tensor ε_{1r} and ε_{1i}) of GGG and Bi:YIGs materials using a combination of ellipsometric and transmission measurements. We used transmission spectra because of the strong interference observed in ψ and Δ in the transparent region bellow 2.5 eV. We fitted the SE experimental data using parametrizations and model structure described above to obtain KK consistent results. We parameterized optical functions of GGG substrate shown in Fig. 1 by Tauc-Lorentz function (1 Tauc-Lorentz oscillator in whole measured spectral range) and optical functions of Bi:YIGs shown in Fig. 2 by Gaussian function (3 Gaussian functions especially in the spectral range 3-5.5 eV) and general Herzinger-Johns function (1 function to parameterize spectra especially bellow 3 eV).
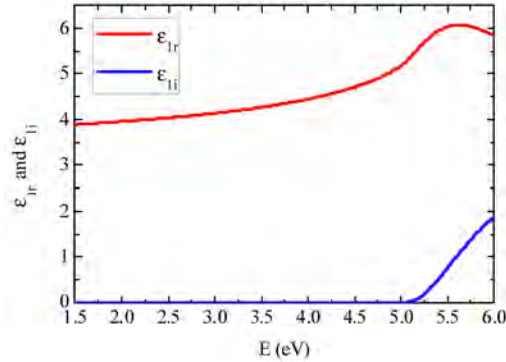
Fig. 1. Spectral dependence of the optical parameters of GGG (100) substrate. The real part ε_{1r} and imaginary part ε_{1i} of the dielectric function is plotted using red and blue lines.
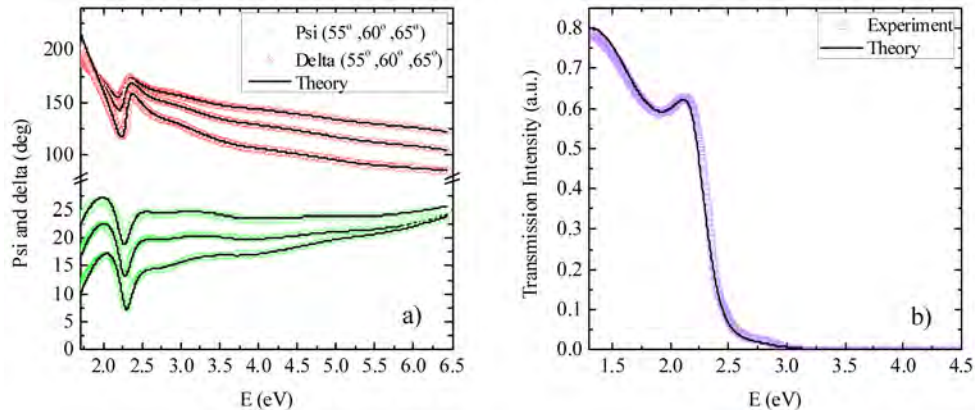
Fig. 2. Experimental data for Bi3YIG layer on GGG substrate compared to the theoretical model (black lines). a) Variable angle SE data. Red and green symbols correspond to measured Psi and Delta respectively. b) Measured spectra of Transmission intensity (purple symbols).

Since substrates were transparent and both-side polished, we considered back reflections in the SE analysis. All thicknesses (including roughness and interface layer) were fitted by the CompleteEase software and subsequently used in MOKE and Faraday spectra analysis. We listed some parameters of used parameterization functions in the Table 2 and the fitted thicknesses in the Table 3.

Table 2. Fitted parameters of Gaussian and Herzinger-Johns functions used to parameterize optical properties of Bi:YIGs layers on GGG substrates in the spectral range 1.5 - 6.5 eV. Here, E_0 stands for central energy of the function; Amp represents amplitude of the function and Br its broadening.

	Gaussian 1			Gaussian 2			Gaussian 3			Herzinger-Johns	
	E_0 (eV)	Amp	Br (eV)	E_0 (eV)	Amp	Br (eV)	E_0 (eV)	Amp	Br (eV)	E_0 (eV)	Amp
Bi3IG	3.27	1.64	0.81	4.36	3.4	1.65	6.27	5.05	3.09	2.60	2.33
Bi2.5YIG	3.2	2.7	1.15	4.33	2.29	1.64	6.51	4.26	3.87	2.49	2.40
Bi2YIG	3.04	1.15	0.77	4.25	1.56	1.68	6.36	2.98	2.37	2.53	1.86
Bi1.5YIG	2.71	0.83	0.46	4.23	0.99	2.19	7.31	2.13	4.18	2.89	1.46

Table 3. Fitted thicknesses and volume fractions used for model of Bi:YIGs layers on GGG substrate in the spectral range 1.5 - 6.5 eV. Here, $T_{Bi:YIG}$ stands for Bi:YIG film thickness; R_{rough} represents film roughness with volume fractions f_{rough}; R_{interf} represents thickness of film/GGG interface with volume fractions f_{interf}.

	$T_{Bi:YIG}$ (nm)	R_{rough} (nm)	f_{rough}	R_{interf} (nm)	f_{interf}
Bi3IG	177	7	0.5	4	0.5
Bi2.5YIG	132	5	0.4	2	0.5
Bi2YIG	165	12	0.6	3	0.5
Bi1.5YIG	175	12	0.5	4	0.5
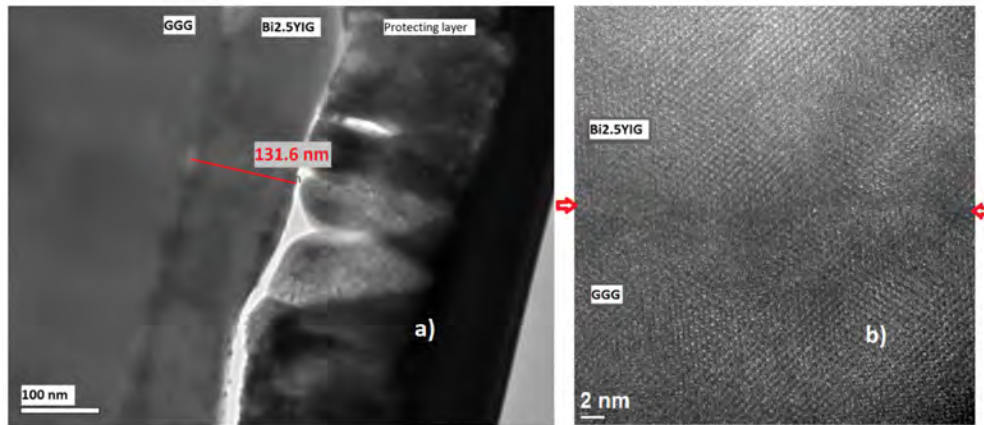
Fig. 3. a) TEM picture of the Bi2.5YIG sample. b) TEM picture of the interface between GGG and Bi2.5YIG layer.

We performed transmission electron microscopy (TEM) measurement on Bi2.5YIG sample. We did this measurement in order to observe the film quality and also to confirm thicknesses derived from SE. Results of the TEM measurement shown in Fig. 3 confirmed that the film was uniform and epitaxially grown on GGG. (This was expected since X-ray diffraction data on different BiYIGs samples grown in our laboratory revealed garnet structure of examined materials [41].) The Fig. 3(a) revealed that the film had a thickness around 132 nm, which is almost 30 nm less that the nominal thickness. In this figure we can also observe interface layer in the form of contrast layer between GGG and Bi2.5YIG, while a magnified TEM image shown in the Fig. 3(b) revealed that Bi2.5YIG has grown epitaxially on GGG substrate. From these results we assumed that the contrast change was caused by slight distortions and stress between adjacent materials. These observations are in a very good

agreement with the SE analysis results (Table 3). We also performed atomic force microscopy roughness measurement on Bi1.5YIG sample. We did this measurement in order to verify relatively high roughness derived from SE. This measurement revealed roughness 11 nm which is also in a good agreement with SE result.

Figures 4 and 5 shows derived spectra of optical parameters ε_{1r} and ε_{1i} for all investigated samples. In the case of ε_{1r} we observed a global maximum around 2.4 eV, local maxima around 3.2 and 4.4 eV and the absorption edge near 2.1 eV. Optical transitions around 2.5, 3.2 and 4.4 eV were also noticeable. Spectra of Bi3YIG and Bi2.5YIG have in the UV region similar shape which is different form the shape of Bi2YIG and Bi1.5YIG. This difference is in a correspondence with the off-diagonal elements of the permittivity tensor spectra (Fig. 5), where we could observe a bigger change in absorption between Bi2YIG and Bi2.5YIG samples. Spectra clearly demonstrated that the bismuth substitution increased amplitudes of ε_{1r} and ε_{1i} in the whole spectral range.

In comparison to previous results on the bulk-like films reported by Wittekoek, in here, we can notice smaller ε_{1i} amplitude and an absorption edge shift from 2.5 to 2.2 eV. However, similar measurement performed on thin single crystal Bi:YIGs films reported absorption data similar to our results [42–44]. Therefore we atributed this disprepancy to the fact that we have been studying thin single crystaline Bi:YIGs films. Previous investigations [8, 45–48] demonstrated that properties of ultra-thin films may significantly differ from properties of thicker films. Difference is ussually caused either by materials' inhomogeneities or, as the thickness of the films decreases, by the increasing influence of surface and interface defective layers (in here modeled by BEMA) [30, 46, 47].
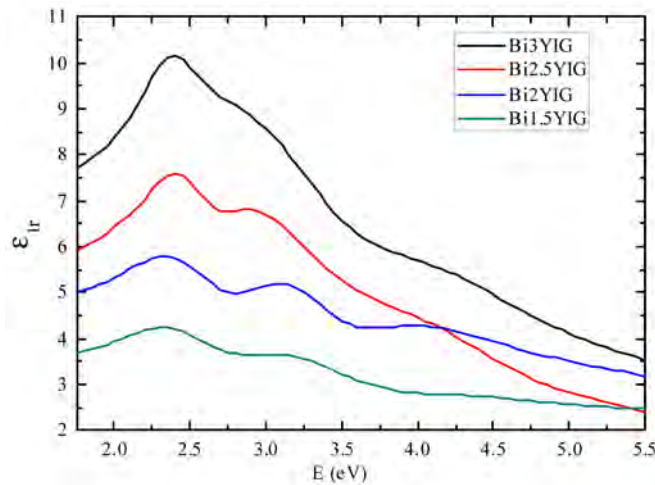
Fig. 4. Real parts of diagonal elements of the permittivity tensor of Bi:YIGs.
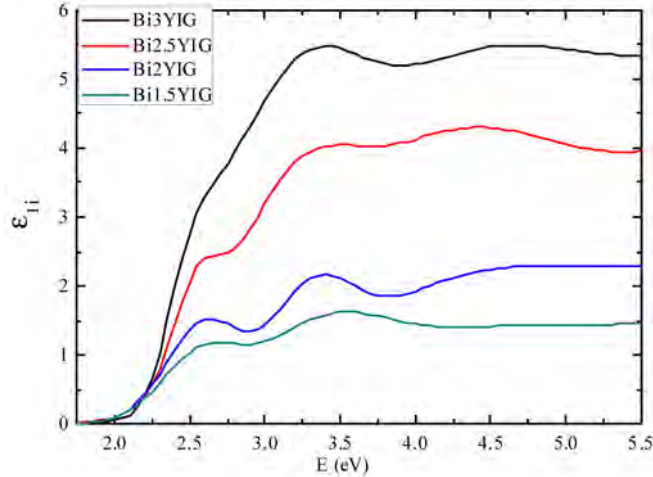
Fig. 5. Imaginary parts of diagonal elements of the permittivity tensor of Bi:YIGs.

4.2 MOKE and Faraday effect spectroscopy

Figure 6(a) shows measured MOKE rotation spectra. Figure 6(b) shows measured MOKE ellipticity spectra. We observed MOKE rotation maxima around 3.4 and 4 eV and MOKE ellipticity maxima near 3.3 and 4.4 eV which is characteristic for Bi:YIGs MOKE spectra [7,9]. Furthermore, we observed strong MO interference in the form of strong oscillations in the spectral range bellow 3 eV. Different interference patterns of samples were caused by theirs different thicknesses. Spectra clearly demonstrated that bismuth substitution increased amplitudes of MOKE rotation and ellipticity effectively.
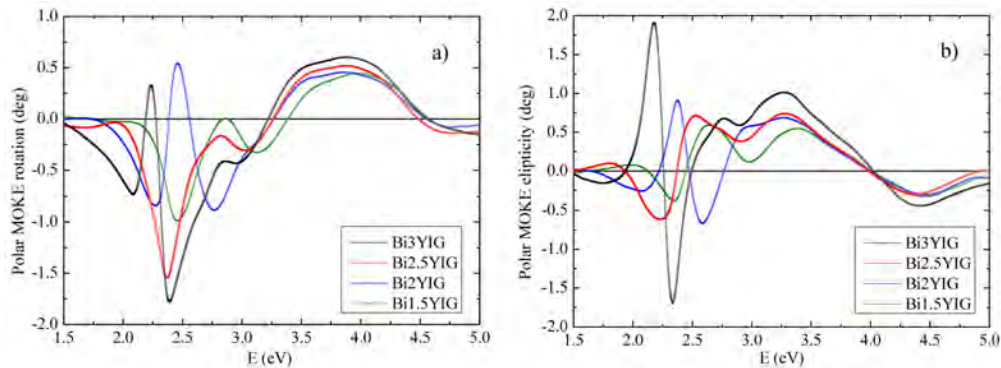
Fig. 6. Polar MOKE a) rotation and b) ellipticity spectra of Bi:YIGs on GGG substrates.

Figure 7(a) shows measured MO Faraday rotation spectra. Figure 7(b) shows measured MO Faraday ellipticity spectra. We corrected experimental data for the rotation from the substrate. We observed Faraday rotation minima near 2.4 eV and two maxima near 2.7 and 3.2 eV. Faraday ellipticity had maxima at 2.7 and minima at 3.3 eV. Spectra clearly demonstrated that bismuth substitution led to the enhancement of the MO Faraday rotation near to 2.4, 2.7 and 3.2 eV and ellipticity near 2.7 eV. Bi substitution also let to an enhancement of MO figure of merit which at 3 eV increased from 4.2° for Bi1.5YIG to 5.1° for Bi3YIG. We demonstrated Faraday rotation angle enhancement by Faraday hysteresis loop measurements shown in Fig. 8.
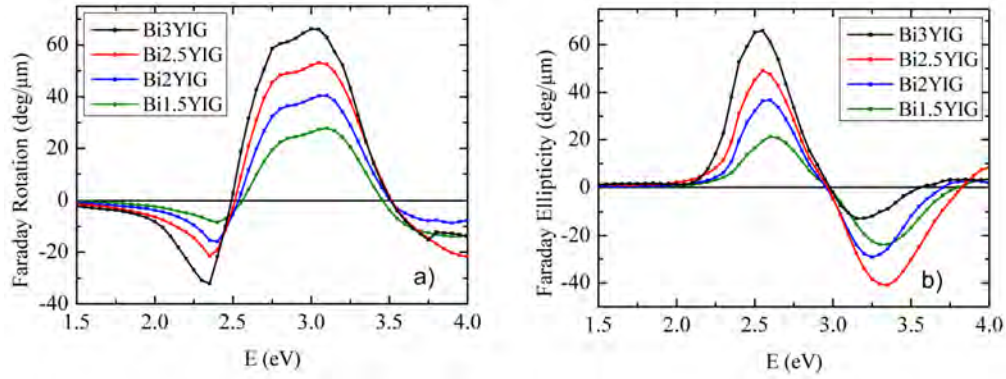
Fig. 7. Faraday effect a) rotation and b) ellipticity spectra of Bi:YIGs on GGG substrates.
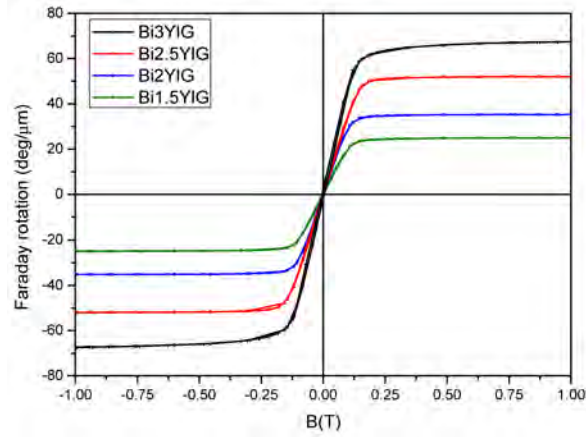
Fig. 8. Faraday rotation hysteresis loops of Bi:YIGs on GGG substrates measured at 3 eV.
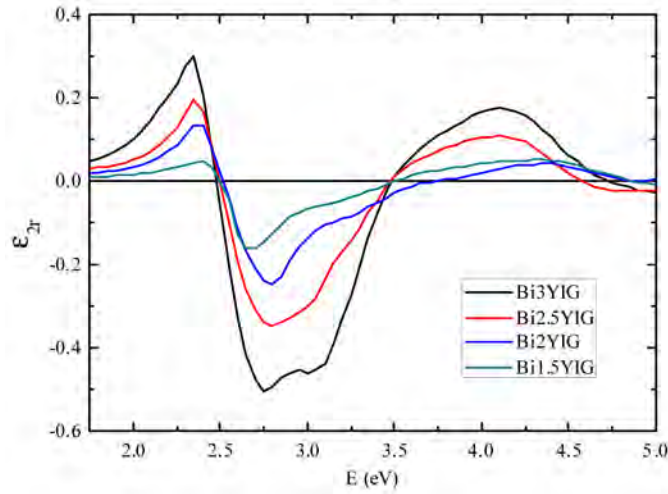
Fig. 9. Real parts of off-diagonal elements of the permittivity tensor of Bi:YIGs.

We calculated the off-diagonal elements of the permittivity tensor ε_{2r} and ε_{2i} from MOKE and Faraday effect spectra using Yeh's 4x4 matrix formalism and diagonal elements of the permittivity tensor determined by SE. Because of the strong MO interference bellow 3 eV we

used MO Faraday effect spectra in the spectral range from 1.5 to 3 eV and MOKE spectra in the spectral range from 3 to 5 eV. Figure 9 shows the real part of off-diagonal permittivity tensor elements ε_{2r} in the whole spectral range. We observed sharp global maxima at 2.4 eV and local maxima 4.2 eV. Transitions on 4.2 eV are most likely due to charge transfers from oxygen to Fe(octahedral) [7]. We also observed minima around 2.7 eV and 3.1 eV especially for higher Bi substitutions. We associated these minima with transitions $t_2(Fe^{3+}) \rightarrow t_{2g}(Fe^{2+})$ and $e_g(Fe^{3+}) \rightarrow e(Fe^{2+})$ which are mainly responsible for the remarkable increase of the Faraday rotation in the visible and near infrared region. Maxima at 2.4 eV are created by the overlap of secondary negative peaks of these two transitions [7]. As expected, bismuth increased ε_{2r} amplitudes at extremes 2.4, 2.7 and 3.1 significantly.

Figure 10 shows the imaginary part of off-diagonal permittivity tensor elements ε_{2i} in the whole spectral range. We observed clear maxima at 2.5 and 4.5 eV and one minimum near 3.4 eV. Spectra demonstrated that bismuth substitution increased amplitudes of ε_{2i}, especially around extremes 2.3, 3.4 and 4.5.
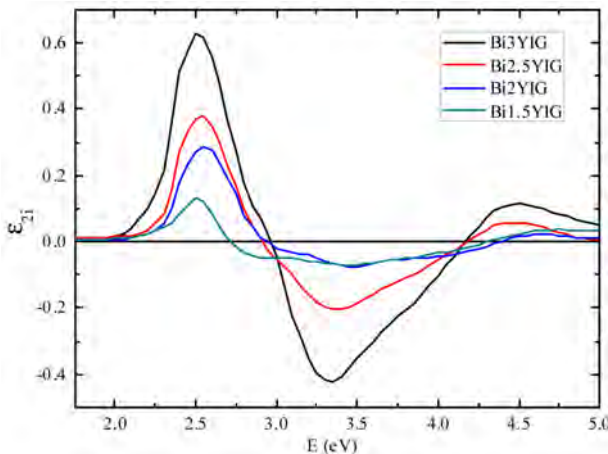
Fig. 10. Imaginary parts of off-diagonal elements of the permittivity tensor of Bi:YIGs.

We would like to note in here that all the calculated permittivity tensor elements spectra have characteristic shape of diagonal and off-diagonal permittivity tensor elements of bulk-like epitaxial Bi:YIGs with small Bi concentrations [7, 9]. We attributed discrepancy to the fact that in this work we characterized epitaxial thin films, which properties may, as explained earlier, differ from the properties of bulk-like materials.

5. Conclusions

In this paper we have presented a systematic optical and MO study of Bi:YIGs thin films prepared by MOD. We have used a combination of SE supported by transmission intensity measurements and MOKE and MO Faraday effect spectroscopy. This combination allowed us to successfully determine the spectral dependence of GGG optical constants and spectral dependence of complete permittivity tensors for Bi:YIGs thin films.

The calculated spectra of diagonal and off-diagonal permittivity tensor elements showed features that are characteristic for bulk-like Bi:YIGs thin films with small Bi concentrations prepared by liquid phase epitaxy [7, 9]. These results therefore confirmed that MOD can be used as an effective technique for the preparation of high optical and MO quality Bi:YIGs thin films with high Bi content.

Acknowledgments